

# Broadband optical absorption enhancement through coherent light trapping in thin-film photovoltaic cells

Mukul Agrawal and Peter Peumans\*

Electrical Engineering, Stanford University, Stanford, CA 94305

\*Corresponding author: [ppeumans@stanford.edu](mailto:ppeumans@stanford.edu)

<http://www.stanford.edu/~ppeumans>

**Abstract:** We show that optical absorption in thin-film photovoltaic cells can be enhanced by inserting a tuned two-component aperiodic dielectric stack into the device structure. These coatings are a generalization and unification of the concepts of an anti-reflection coating used in solar cells and high-reflectivity distributed Bragg mirror used in resonant cavity-enhanced narrowband photodetectors. Optimized two-component coatings approach the physically realizable limit and optimally redistribute the spectral photon density-of-states to enhance the absorption of the active layer across its absorption spectrum. Specific designs for thin-film organic solar cells increase the photocurrent under AM1.5 illumination, averaged over all incident angles and polarizations, by up to 40%.

©2008 Optical Society of America

**OCIS codes:** (310.6845) Thin film devices and applications; (230.5170) Photodiodes; (160.4890) Organic materials; (030.1670) Coherent optical effects; (310.4165) Multilayer design.

---

## References and links

1. S. R. Forrest, "The path to ubiquitous and low-cost organic electronic appliances on plastic," *Nature* **428**, 911-918 (2004).
2. D. Redfield, "Multiple-pass thin-film silicon solar cell," *Appl. Phys. Lett.* **25**, 647-648 (1974).
3. P. Campbell and M. A. Green, "Light trapping properties of pyramidally textured surfaces," *J. Appl. Phys.* **62**, 243-249 (1987).
4. T. Tiedje, E. Yablonovitch, G. D. Cody and B. G. Brooks, "Limiting efficiency of silicon solar cells," *IEEE Trans. Electron. Devices* **ED-31**, 711-716 (1984).
5. P. Peumans, A. Yakimov, and S. R. Forrest, "Small molecular weight organic thin-film photodetectors and solar cells," *J. Appl. Phys.* **93**, 3693-3723 (2003).
6. L. S. Roman, O. Inganäs, T. Granlund, T. Nyberg, M. Svensson, M. R. Andersson and J. C. Hummelen, "Trapping light in polymer photodiodes with soft embossed gratings," *Adv. Mater.* **12**, 189-195 (2000).
7. E. Yablonovitch, "Statistical ray optics," *J. Opt. Soc. Amer.* **72**, 899-907 (1982).
8. H. Stiebig, N. Senoussaoui, C. Zahren, C. Haase, and J. Müller, "Silicon thin-film solar cells with rectangular-shaped grating couplers," *Prog. Photovoltaics* **14**, 13-24 (2006).
9. P. Peumans and S. R. Forrest, "Very-high-efficiency double-heterostructure copper phthalocyanine/C60 photovoltaic cells," *Appl. Phys. Lett.* **79**, 126-128 (2001).
10. P. Peumans, S. Uchida, and S. R. Forrest, "Efficient bulk heterojunction photovoltaic cells using small-molecular-weight organic thin films," *Nature* **425**, 158-162 (2003).
11. J. Xue, B. P. Rand, S. Uchida, and S. R. Forrest, "A hybrid planar-mixed molecular heterojunction photovoltaic cell," *Adv. Mater.* **17**, 66-71 (2005).
12. G. Li, V. Shrotriya, J. Huang, Y. Yao, T. Moriarty, K. Emery, and Y. Yang, "High-efficiency solution processable polymer photovoltaic cells by self-organization of polymer blends," *Nat. Mater.* **4**, 864-868 (2005).
13. W. Ma, C. Yang, X. Gong, K. Lee, and A. J. Heeger, "Thermally stable, efficient polymer solar cells with nanoscale control of interpenetrating network morphology," *Adv. Funct. Mater.* **15**, 1617-1622 (2005).
14. P. Sheng, A. N. Bloch, and R. S. Stepleman, "Wavelength-selective absorption enhancement in thin-film solar cells," *Appl. Phys. Lett.* **43**, 579-581 (1983).
15. J. Zhao and M. A. Green, "Optimized antireflection coatings for high-efficiency silicon solar cells," *IEEE Trans. Electron. Devices* **38**, 1925-1934 (1991).

16. R. R. Bilyalov, L. Stalmans, L. Schirone, and C. Levy-Clement, "Use of porous silicon antireflection coating in multicrystalline silicon solar cell processing," *IEEE Trans. Electron. Devices* **46**, 2035-2040 (1999).
17. L. A. A. Pettersson, L. S. Roman, and O. Inganas, "Modeling photocurrent action spectra of photovoltaic devices based on organic thin film," *J. Appl. Phys.* **86**, 487-496 (1999).
18. K. Kishino, M. S. Unlu, J. Chyi, J. Reed, L. Arsenaault, and H. Morkoc, "Resonant cavity-enhanced photodetector," *IEEE J. Quantum Electron.* **27**, 2025-2034 (1991).
19. M. S. Unlu and S. Strite, "Resonant cavity enhanced photonic devices," *J. Appl. Phys.* **78**, 607-639 (1995).
20. L. Brillouin, *Wave Propagation and Group Velocity* (Academic Press, 1960).
21. C. W. Tang, "Two layer organic photovoltaic cell," *Appl. Phys. Lett.* **48**, 183-185 (1986).
22. P. Yeh, *Optical Waves in Layered Media* (John Wiley & Sons, 1998).
23. M. A. Dupertuis, B. Acklin and M. Proctor, "Generalized energy balance and reciprocity relations for thin film optics," *J. Opt. Soc. Am. A* **11**, 1167-1174 (1994).
24. R. J. Vernon and S. R. Seshadri, "Reflection coefficient and reflected power on a lossy transmission line," *Proc. IEEE*, **57**, 101-102 (1969).
25. G. P. Ortiz and W. L. Mochan, "Nonadditivity of Poynting vector within opaque media," *J. Opt. Soc. Am. A* **22**, 2827-2837 (2005).
26. J. S. Toll, "Causality and the dispersion relation: logical foundations," *Phys. Rev.* **104**, 1760-1770 (1956).
27. H. M. Nussenzveig, *Causality and Dispersion Relations* (Academic, 1972).
28. V. Lucarini, J. J. Saarinen, K.-E. Peiponen, and E. M. Vartiainen, *Kramers-Kronig Relations in Optical Materials Research*, (Springer, 2005).
29. E. C. Titchmarsh, *Introduction to the Theory of Fourier Integrals* (Oxford, 1948).
30. A. V. Tikhonravov, P. W. Baumeister, and K. V. Popov, "Phase properties of multilayers," *Appl. Opt.* **36**, 4382-4392 (1997).
31. G. Lenz, B. J. Eggleton, C. R. Giles, C. K. Madsen, and R. E. Slusher, "Dispersive properties of optical filters for WDM systems," *IEEE J. Quantum Electron.* **34**, 1390-1402 (1998).
32. R. K. Ahrenkiel, "Modified Kramers-Kronig analysis of optical spectra," *J. Opt. Soc. Am.* **61**, 1651-1655 (1971).
33. C. A. Emeis, L. J. Oosterhoff, and G. de Vries, "Numerical evaluation of Kramers-Kronig Relations," *Proc. R. Soc. Lond. A* **297**, 54-65 (1967).
34. K. Tvingstedt, V. Andersson, F. Zhang, and Olle Inganas, "Folded reflective tandem polymer solar cell doubles efficiency," *Appl. Phys. Lett.* **91**, 123514-1-123514-3 (2007).
35. A. V. Tikhonravov, "Some theoretical aspects of thin-film optics and their applications," *Appl. Opt.* **32**, 5417-5426 (1993).
36. B. T. Sullivan and J. A. Dobrowolski, "Implementation of a numerical needle method for thin-film design," *Appl. Opt.* **35**, 5484-5492 (1996).
37. A. V. Tikhonravov, M. K. Trubetskov, and G. W. DeBell, "Application of the needle optimization technique to the design of optical coatings," *Appl. Opt.* **35**, 5493-5508 (1996).
38. M. Agrawal and P. Peumans, "Design of non-periodic dielectric stacks for tailoring the emission of organic light-emitting diodes," *Opt. Express* **15**, 9715-9721 (2007).
39. M. Agrawal, Y. Sun, S. R. Forrest, and P. Peumans, "Enhanced outcoupling from organic light-emitting diodes using aperiodic dielectric mirrors," *Appl. Phys. Lett.* **90**, 241112-1-241112-3 (2007).
40. J. A. Nelder and R. Mead, "Simplex method for function minimization," *Comput. J.* **7**, 308-313 (1965).
41. Matlab 7.0, The Mathworks Inc., Apple Hill Drive, Natick, MA 01760.
42. B. O'Connor, K. H. An, K. Pipe, Y. Zhao, and M. Shtein, "Enhanced optical field intensity distribution in organic photovoltaic devices using external coatings," *Appl. Phys. Lett.* **89**, 233502 (2006).

Thin-film photovoltaic (PV) cells may provide for our energy needs at a price that is competitive with grid power [1]. However, significant improvements in cost per peak Watt are still required to reach grid parity. This can be achieved by increasing the efficiency or reducing the manufacturing cost. The efficiency of a PV cell depends on the likelihood that an incident photon is absorbed and the efficiency of the subsequent conversion of the photon into electrical energy. The photon absorption probability improves as the thickness of the active material is increased. At the same time, the probability that the absorbed energy is collected as electrical energy at the electrodes reduces as the active layer thickness is increased due to enhanced recombination [2]-[6]. Light trapping [2]-[8] addresses this fundamental trade-off by increasing the optical absorption of a given active layer thickness.

A well-known and effective light trapping approach is to use geometric Lambertian scattering [7] at one or both surfaces bounding the absorbing layer [Fig. 1(a)]. This approach increases the absorption by randomizing the occupation of the photon density-of-states (PDOS) [7]. Since this approach is based on the principles of statistical ray optics [7], it only applies to PV cells whose active layer thickness is much larger than the wavelength. Thin-film PV cells have film thicknesses that are similar to or smaller than the wavelength [8]-[13]. For example, in organic PV cells, the optimal active layer thickness is 20nm-200nm [9]-[13]. In

this case, subwavelength structures can be used to redistribute the PDOS from spectral regions where absorption is sufficiently strong or not needed to spectral regions where absorption enhancement would lead to enhanced photocurrents [6]-[8], [14]. Recently, the use of embossed gratings to scatter incident light into guided modes in polymer PV cells with active layer thicknesses <100nm was explored [6]. A maximum increase in external quantum efficiency of 30% was observed at a wavelength of  $\lambda=420\text{nm}$  [6], while the short-circuit current under AM1.5 illumination was enhanced by <10%.

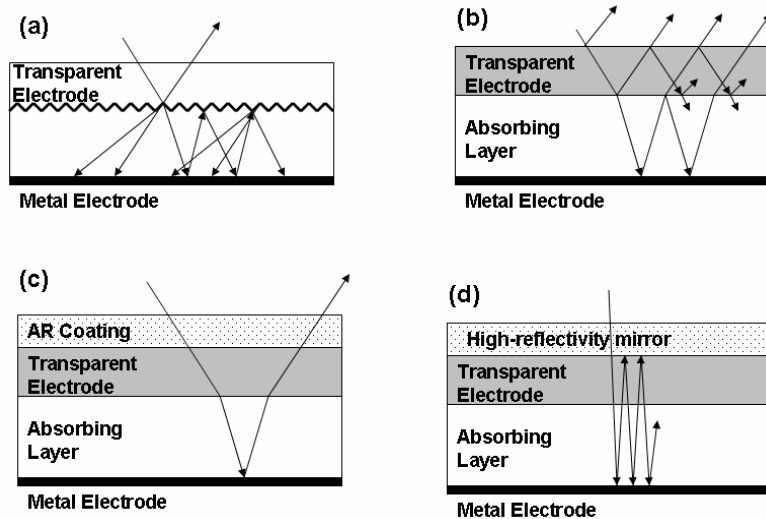


Fig. 1. Simplified schematics of thin film PV cells (a) with Lambertian scattering at the transparent electrode interface, (b) without an ARC, (c) with an ARC over the transparent electrode, and (d) with a high-reflectivity mirror over the transparent electrode in the RCE configuration.

In this Letter, we evaluate a light trapping scheme for thin film PV cells that uses tailored dielectric mirrors to build broadband cavities that maximize solar spectral harvesting. Using the example of an organic PV cell, we show that the short circuit current can be enhanced by 40% for a broadband organic absorber, demonstrating that light trapping methods that rely on modifying the PDOS have considerable merit for thin-film PV cells. The dielectric mirrors are a generalization of the concepts of an anti-reflection coating (ARC) and distributed Bragg reflector (DBR).

A simplified schematic of a PV cell in which a semiconductor is sandwiched between a transparent electrode and a reflecting metal electrode is shown in Fig. 1(b). Due to differences in refractive index of the different layers, a fraction of the incident light is reflected away from the device at one of the various entrance interfaces. The remaining light has multiple chances of being absorbed in the active layer as it makes round trips between the bottom mirror formed by the reflecting metal electrode and mirror formed by the multiple interfaces between the absorbing layer and air. Dielectric ARCs [Fig. 1(c)] have found widespread use to reduce reflection losses in PV cells [15]-[16]. Since an ARC reduces the air-to-absorbing-layer reflectivity, it also prevents the optical energy from making multiple round trips inside the absorbing layer. Even though the probability of multiple round trips reduces, in the limit of geometric optics (active layer thickness  $L \gg \lambda$ ), one always benefits from using an ARC. Summing the multi-trip absorption (ignoring optical interference effects) for a structure with an ideal reflector on the backside (bottom mirror), one obtains that the ratio of the absorption efficiency of a structure with a perfect ARC over that of one without an ARC is

$$\frac{1 - R_1 \exp(-2\alpha L)}{(1 - R_1)}. \text{ Here, } R_1 \text{ is the reflectivity from air into the active layer without ARC}$$

and  $\alpha$  is the absorption coefficient of the active layer. ARCs always improve the absorption efficiency when  $L \gg \lambda$  even though its utility is lost for weak absorbers ( $\alpha L \rightarrow 0$ ).

On the other hand, in thin-film PV cells, where the thickness of the absorbing layer is smaller than or similar to the wavelength, optical interference effects are significant and can be exploited to improve the optical absorption [5], [17]. High-reflectivity dielectric mirrors [Fig. 1(d)] are commonly used in resonant cavity-enhanced (RCE) photodetectors [18]-[19] to enhance the absorption over a narrow spectral and angular range using constructive interference. An approximate but simple analysis [18]-[19] that neglects the standing wave effects predicts that the peak absorption enhancement at the resonant wavelength for a

structure with ideal bottom reflector is  $\frac{(1-R_1)}{(1-\sqrt{R_1} \exp(-\alpha L))^2}$ . A more accurate and

detailed analysis is discussed below. The enhancement is evaluated with respect to a structure bounded by a perfect ARC and ideal reflector. The resonant wavelength is determined by the resonance condition:

$$\frac{2n_N \omega L}{c} + \phi_1 + \phi_2 = 2m\pi \quad (1)$$

where  $\phi_1$  and  $\phi_2$  are the phase change upon reflection from the top and bottom mirrors,  $\omega$  is the frequency,  $n_N$  is the real part of the refractive index of the active layer,  $c$  is the speed of light, and  $m$  is a positive integer. Maximum resonant enhancement of the optical absorption is achieved when the entrance mirror is “impedance matched” to the absorber:  $R_1 = \exp(-2\alpha L)$ . In RCE structures, the dielectric mirrors are usually configured as high reflectivity DBRs such that constructive interference is obtained in the active layer for a narrow spectral and angular range because the phase of the reflectivity from these mirrors is correct only for those conditions [18]-[19].

We now explore whether the concepts of an ARC and mirrors for RCE structures can be unified to the concept of a mirror that maximizes the optical absorption in a thin-film solar cell across its absorption spectrum. Such a mirror needs to exhibit a high reflectivity in the spectral range where the active layer is a weak absorber to enhance absorption through constructive interference, and a low reflectivity where the active layer is a strong absorber to operate as an ARC. In the high-reflectivity regions of the spectrum, the mirror needs to have an anomalous (negative) phase dispersion: the phase upon reflection,  $\phi_1$ , needs to decrease with frequency  $\omega$ , following Eq. (1). Broadband anomalous phase dispersion would violate causality, and would mean superluminal group and front velocity [20] and is therefore not physically realizable. Trade-offs are therefore necessary.

We first develop a detailed model for two types of organic thin-film PV cells to evaluate the dependence of short-circuit current under AM1.5 illumination on the spectral properties, i.e. reflectivity,  $R_1(\omega)$ , and phase,  $\phi_1(\omega)$ , of the top mirror. We then study the upper bound on the short-circuit current enhancement imposed by the requirement that the mirror characteristics are causal. Finally, we provide a practical numerical optimization scheme to design multilayer dielectric stacks with a performance that approaches the causal limits and provide two example designs that increase the photocurrent of a thin-film organic solar cell by up to 40%.

A schematic of a general thin-film PV cell on a transparent substrate and with a reflective back electrode is shown in Fig. 2. Layer  $N$  is the active layer for which we want to enhance the optical absorption. Layer 1 (transparent substrate) and layer  $M$  (metal electrode) are assumed to be semi-infinite. The active (absorbing) layer can be thought of as bounded between two mirrors. The top mirror is formed by the transparent electrode, sequence of dielectric layers, and substrate, while the bottom mirror is formed by a spacer layer and metal electrode. All interfaces are assumed to be optically flat. Light is incident from layer 1 at an arbitrary angle with mixed s- and p-polarization. It is assumed that the absorbing layer produces electrons and holes. One carrier type is collected by the transparent electrode, while the other type is transported to the metal electrode via the spacer layer. For our analysis, we focus on organic donor-acceptor (DA) solar cells with an active layer consisting of either a nanostructured bulk heterojunction (BHJ) of the electron acceptor 3,4,9,10 perylene tetracarboxylic bisbenzimidazole (PTCBI) and donor copper phthalocyanine (CuPc) [10], or a CuPc/PTCBI bilayer [21]. The layer structures of the PV cells investigated are glass/100nm ITO/15nm CuPc:PTCBI (1:1 weight ratio)/20nm bathocuproine (BCP)/Al for the BHJ device and glass/100nm ITO/11.5nm CuPc/3.5nm PTCBI/20nm BCP/Al for the bilayer device. Note that very thin active layers (15nm) are used since light trapping is more useful for such structures. The BCP layer functions as a transparent spacer layer that transports electrons to the Al cathode [9]. The wavelength-dependent complex refractive indices of CuPc, PTCBI and Al were measured by spectroscopic ellipsometry. Dispersion in glass, ITO, BCP and the dielectric coating materials  $\text{SiO}_2$  and  $\text{TiO}_2$  was ignored. The refractive indices of all materials at  $\lambda=600\text{nm}$  are tabulated in Table 1.

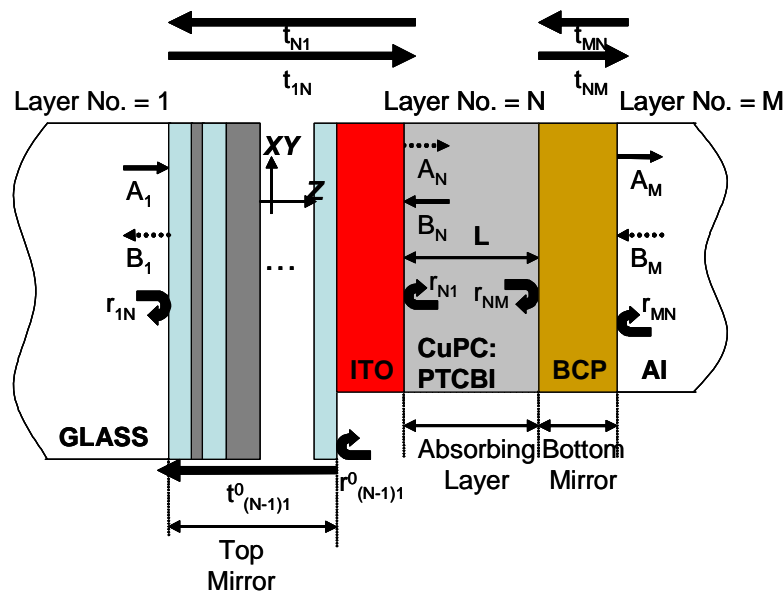


Fig. 2. Schematic of a thin-film organic PV cell with an aperiodic dielectric stack between the glass substrate and transparent ITO anode.

In the bilayer PV cell with the DA interface at  $z = z_0$  and a total active layer thickness of  $L$ , the exciton flux at the DA interface as a function of the angle of incidence  $\theta$  with respect to the substrate normal can be written as

Table 1. The refractive indices of all materials at  $\lambda=600\text{nm}$  in the multilayer BHJ and bilayer cell designs.

Bilayer Design				BHJ Design			
Layer No.	Material	Thickness(nm)	Refractive Index at 600nm	Layer No.	Material	Thickness(nm)	Refractive Index at 600nm
	glass		1.5		glass		1.5
1	TiO <sub>2</sub>	10.41	2.5	1	TiO <sub>2</sub>	12.94	2.5
2	SiO <sub>2</sub>	66.23	1.5	2	SiO <sub>2</sub>	45.46	1.5
3	TiO <sub>2</sub>	10.92	2.5	3	TiO <sub>2</sub>	67.33	2.5
4	SiO <sub>2</sub>	208.56	1.5	4	SiO <sub>2</sub>	16.5	1.5
5	TiO <sub>2</sub>	66.76	2.5		ITO	100	1.9+0.05i
6	SiO <sub>2</sub>	20.09	1.5		CuPc:		
	ITO	100	1.9+0.05i		PTCBI	15	1.85+0.85i
	CuPc	11.5	1.8+0.89i		BCP	20	1.7
	PTCBI	3.5	1.9+0.81i		Al		1.2+7.33i
	BCP	20	1.7				
	Al		1.2+7.33i				

$$j_{exciton}(\theta) = \sum_{s,p} \int_0^L \int_0^L G_{s,p}(z, \omega, \theta) f(z) dz d\omega \quad (2)$$

Here  $G_{s,p}(z, \omega, \theta)$  is the exciton generation rate as a function of location in the active layer,  $z$ , wavelength,  $\lambda=2\pi c/\omega$ , the angle of incidence,  $\theta$  and the optical polarization ( $s$  or  $p$ ).

$f(z) = \frac{\partial G(z, z')}{\partial z'} \Big|_{z'=z_0}$  is the exciton collection efficiency, where  $G(z, z')$  is the Green's

function for the exciton transport equation  $-D_p \frac{\partial^2 G(z, z')}{dz'^2} - \frac{G(z, z')}{\tau_p} = \delta(z' - z)$  with the

boundary conditions  $G(z_0, z') = 0$  (complete quenching at the DA interface) and

$\frac{\partial G(z, z')}{\partial z'} \Big|_{z=0 \text{ or } L} = 0$  (no exciton quenching at the other interfaces). Here,  $\delta(z' - z)$  is the

Dirac delta function centered at  $z$ , and  $D_p$  and  $\tau_p$  are the exciton diffusivity and lifetime, respectively. Charge carriers are generated by exciton dissociation at the DA interface. It should be stressed that the Green's function approach to the solution of exciton diffusion equation containing a position dependent exciton source term provides significant computational benefit by avoiding a more commonly used finite difference approach to solve the inhomogeneous differential equation for each tested mirror structure after evaluating interference pattern for each such structures.

The BHJ solar cell is also described by Eq. (2) but exciton collection is assumed to be 100% efficient:  $f(z) \approx 1$ . We assume an exponentially decaying probability for the collection efficiency of charge carriers at the electrodes. The short-circuit photocurrent density,  $j_{sc}(\theta)$ , is then equal to  $e j_{exciton}(\theta) \exp(-L/L_c)$  where  $e$  is the electronic charge and the carrier collection length,  $L_c$ , is a parameter that depends on the choice of material and processing conditions used.

The exciton generation rate,  $G_{s,p}(z, \omega, \theta)$ , strongly depends on optical interference effects and is given by

$$G_{s,p}(z, \omega, \theta) = \frac{n_i'(\omega)\alpha_i(\omega)}{n_i(\omega)\hbar\omega} I(\omega, \theta) |\mathbf{E}_{s,p}(z, \omega, \theta)|^2 \quad (3)$$

where  $I(\omega, \theta)$  is incident solar power spectral density per unit projected area as a function of azimuthal angle,  $\theta$ .  $\mathbf{E}_{s,p}(z, \omega, \theta)$  is the relative electric field with respect to the incident electric field and  $n_i'$  and  $\alpha_i$  are the real part of the refractive index and absorption coefficient, respectively, of the  $i^{\text{th}}$  layer. The change in solar power flux as a function of angle is assumed to follow the cosine law:  $I(\omega, \theta) = I_0(\omega) \cos(\theta)$ . Modeling the top and the bottom mirrors as two-port linear systems, one can calculate the electric field inside the absorbing layer in terms of the two-sided scattering coefficients of both mirrors:

$$\mathbf{E}_s(z, \omega, \theta) = \frac{t_{1N} \exp(ik_{zN}z) + r_{NM} t_{1N} \exp(2ik_{zN}L - z)}{1 - r_{N1} r_{NM} \exp(2ik_{zN}L)} \hat{\mathbf{e}}_s \quad (4)$$

$$\mathbf{E}_p(z, \omega, \theta) = \frac{k_N}{\epsilon_N \omega} \frac{t_{1N} \exp(ik_{zN}z) \hat{\mathbf{e}}_{p,+} + r_{NM} t_{1N} \exp(2ik_{zN}L - z) \hat{\mathbf{e}}_{p,-}}{1 - r_{N1} r_{NM} \exp(2ik_{zN}L)} \quad (5)$$

Here,  $\hat{\mathbf{e}}_s = \hat{\mathbf{z}} \times \hat{\mathbf{k}}_{xy}$  and  $\hat{\mathbf{e}}_{p,\pm} = (-k_{zN} \hat{\mathbf{k}}_{xy} \pm k_{xy} \hat{\mathbf{k}}_{zN}) / k_N$  are unit vectors and  $k_{zN} = k_{zN}' + ik_{zN}''$  and  $k_{xy}$  are the transverse and in-plane components of the wave vector  $k_N$  in the absorbing layer.  $\epsilon_N$  is the permittivity of the absorbing layer and  $z$  is the distance from the interface of the absorber and the transparent electrode.  $r_{ij}$  and  $t_{ij}$  are the complex Fresnel scattering coefficients [22] as shown in Fig. 2.

Noting that the transmissivities from two sides for any arbitrary layer structure are related [23] as  $t_{1N} = t_{N1} k_{z1} / k_{zN}$ , Eqs. (2)-(5) parameterize the performance of a thin-film PV cell in terms of three optical scattering parameters  $|t_{N1}|$ ,  $r_{N1}$ , and  $r_{NM}$ . This parametric model thus enables us to search for the optimally desired mirror characteristics independent of any particular physical construction of the mirrors such as layer thicknesses and their refractive indices. Two of these,  $t_{N1}$  and  $r_{N1}$ , are constrained through conservation of energy and are therefore not independent parameters. In thin layers of strong absorbing media, plane waves are inhomogeneous waves and thus some care is required [24]-[25] when enforcing energy conservation relation between  $t_{N1}$  and  $r_{N1}$ . Instead of using  $r_{N1}$ , we find that the magnitude and phase of the reflectivity  $r_{(N-1)1}^0 = R \exp(i\phi)$  of light incident from air on the mirror deposited on the substrate (see Fig. 2) are more convenient parameters to describe the top mirror. It should be noted that while  $|r_{(N-1)1}^0| = R \leq 1$ , such an assertion can not be made about  $|r_{N1}|$  [24]-[25]. An easily enforced bound on  $R$  and  $\phi$  simplifies locating the optimal spectral profile of the mirror characteristics. Since the substrate and the dielectrics in the mirror stack are assumed lossless, one can enforce conservation of energy between transmissivity  $t_{(N-1)1}^0$  and reflectivity  $r_{(N-1)1}^0 = R \exp(i\phi)$  by requiring that

$|t_{(N-1)l}^0|^2 = (1 - |r_{(N-1)l}^0|^2) k_{z0}' / k_{z1}'$  which then can be propagated [22] to evaluate  $t_{N1}$  and  $r_{N1}$ , respectively. Hence, the top mirror (including a lossy anode) can be parameterized in terms of  $R$  and  $\phi$ .

We first ignore the constraint between  $R$  and  $\phi$  that is imposed by the requirement that the mirror response be causal and determine for each wavelength,  $\lambda$ , the desired  $R$  and  $\phi$  that maximize the spectral absorbance given by:

$$\eta_{s,p}(\omega) = \frac{\hbar\omega}{I(\omega, \theta)} \int_0^L G_{s,p}(z, \omega, \theta) dz \quad (6)$$

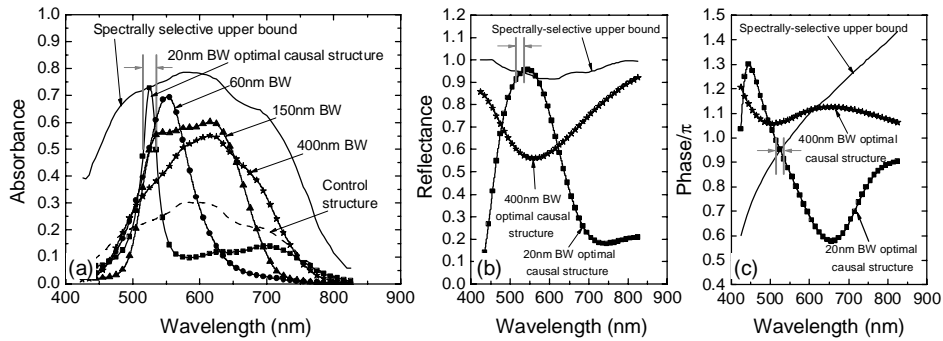


Fig. 3. (a). Absorbance as a function of wavelength is shown for a device with 15nm thick active layer (control structure) without a multilayer mirror (dashed line). Also shown are the spectrally-selective upper bound of absorbance (solid line) and the absorbance of devices with optimal causal top mirror such that the AM 1.5 weighted average EQE over different target wavelength bandwidths (BW) is maximized (squares: BW=20nm, circles: BW=60nm, triangles: BW=150nm, stars: BW=400nm). (b) shows the corresponding amplitude of reflectance of the top mirror and (c) shows the corresponding phase of reflectance of the top mirror to achieve the spectrally selective-upper bound (solid line). The desired amplitude and phase of reflectance for causal top mirrors designed for broadband (BW=400nm, stars) and narrowband (BW=20nm, squares) response are also shown.

Because this absorbance can be achieved in a physically realizable device only over a narrow frequency range, we refer to this as the spectrally-selective upper bound. Figure 3(a) shows the spectrally-selective upper bound for the spectral absorbance of a CuPc:PTCBI BHJ device with 15nm-thick active layer (solid line) and compares it to that of the unmodified device structure (dashed line). The desired  $R$  (Fig. 3(b), solid line) of the mirror is lowest in the spectral range where the absorption strength  $\alpha_N L$  is largest. Strong absorption eliminates the possibility of multiple bounces of the light such that a lower  $R$  is more desirable to enhance the incoupling of light by working as an ARC. The ideal  $\phi$  shows anomalous phase dispersion across the full spectrum (Fig. 3(c), solid line).

As noted above, this spectrally-selective upper-bound cannot be approached over a large bandwidth. For any physically realizable mirror, the time impulse plane wave reflectivity  $\tilde{r}_{(N-1)l}^0(t)$  must be a causal [26]-[29] and bounded function [24]-[25]. This ensures that the spectral reflectivity  $r_{(N-1)l}^0(\omega)$  of the mirror is an analytic function [26]-[27] in the lower half of the complex frequency plane while, on the real frequency axis,  $\text{Re}\{r_{(N-1)l}^0(\omega)\}$  and

$\text{Im}\{r_{(N-1)1}^0(\omega)\}$  are related by the generalized dispersion relations [27]-[28]. In other words, the poles of  $r_{(N-1)1}^0(\omega)$  lie in the upper half complex plane while its zeros can lie in both the upper and lower halves [30]-[31]. For broadband enhancement of absorbance, mirrors with broadband negative phase dispersion are required. Since zeros in the lower half complex plane contribute to monotonic positive phase dispersion while zeros in the upper half contribute to the monotonic negative phase dispersion [30]-[31], a minimum-phase system [26],[31] with all its zeros in the upper half plane is most appropriate for coherent light trapping. For a minimum-phase system,  $\log(r_{(N-1)1}^0(\omega)) = \log(R(\omega)) + i\phi(\omega)$  is analytic in the lower half space and a generalized dispersion relation known as the singly-substituted Kramers-Kronig (SSKK) relation with substitution frequency of  $\omega_1 = 0$  can be written between  $\log(R(\omega))$  and  $\phi(\omega)$  [27]-[28], [32]:

$$\phi(\omega) = -\frac{2\omega}{\pi} \int_0^{\infty} \frac{\log(R(\omega'))}{\omega'^2 - \omega^2} d\omega' + \phi(0) \quad (7)$$

Here, the long-wavelength asymptotic value [28] of reflectivity is taken to be  $r_{(N-1)1}^0(0) = \frac{n_1 - 1}{n_1 + 1}$  since the optical effects of the multilayer coatings become negligible at very long wavelengths. We have developed a perturbative method that starts from a trivial

SSKK-consistent combination of  $R(\omega) = \left| \frac{n_1 - 1}{n_1 + 1} \right|$  and  $\phi(\omega) = \arg\left(\frac{n_1 - 1}{n_1 + 1}\right)$  and gradually

builds another SSKK-consistent pair ( $R(\omega)$  and  $\phi(\omega)$ ) on a discrete frequency grid  $\{\omega_j\}$ , that maximizes the short-circuit current under AM1.5 illumination in the device geometry shown in Fig. 2. The kernel of the integral in Eq. (7) is sharply peaked around  $\omega = \omega'$ . Therefore, for each discretized value of frequency,  $\omega_j$ , the values of reflectance  $R(\omega_j)$  at  $p$  neighboring  $\omega_j$  (typically  $p=5-7$ ) are simultaneously perturbed within a small range (typically  $\pm 0.01$  in  $q=10$  discrete steps). For each of the  $p^q$  spectral profiles,  $R(\omega_j)$ , the corresponding causal conjugate,  $\phi(\omega_j)$ , is constructed using Eq. (7). The short-circuit current under 1 sun AM1.5 illumination is then evaluated using Eqs. (2)-(5) for each of the  $p^q$  pairs of  $R(\omega_j)$  and  $\phi(\omega_j)$  and the optimal pair is retained. This procedure is repeated for every discretized frequency  $\omega_j$ . Once a full scan is complete, a 15<sup>th</sup> degree polynomial is fitted to  $R(\omega)$ . This complete procedure is repeated until no further improvements are obtained. The integral in Eq. (7) is evaluated numerically [33] over a frequency range that is several times larger (typically 5-13 times) than the frequency bandwidth over which absorption enhancement is desired. This reduces the numerical errors inside range of interests and also allows ample opportunity for the reflectance  $R(\omega)$  to change outside the range of interest such that both  $R(\omega)$  and  $\phi(\omega)$  can approach the desired values in the frequency range of interest. For the purpose of studying causality imposed upper limit on the achievable solar photovoltaic conversion through planar coherent light trapping, we restricted ourselves to the case normal incidence of light.

The optimized SSKK-consistent limits for the absorption of a BHJ device structure when absorption enhancement is desired over a bandwidth ranging from 20nm to 400nm, is shown in Fig. 3(a). These results were obtained by optimizing the mirror characteristics subject to the SSKK for maximum photocurrent of the solar cell as discussed above while limiting the incident spectrum to a spectral band  $\lambda=515\text{nm}-(515\text{nm}+\Delta)$  with  $\Delta=20\text{nm}$  (squares), 60nm (circles), 150nm (triangles). Also shown is the KK-consistent limit for the full absorption

band  $\lambda=425\text{nm}-825\text{nm}$  (stars). The KK-consistent search results in a reflectance amplitude [Fig. 3(b)] and phase [Fig. 3(c)] profile that is similar to that of a DBR when absorption enhancement is desired over  $\Delta=20\text{nm}$  (squares). In this case, the enhancement reaches the spectrally-selective upper-bound [Fig. 3(a)]. On the other hand, for PV applications, where broadband absorption enhancement is desired, negative phase dispersion is required as seen in Fig. 3(c) (stars) and it is not possible to reach the spectrally-selective upper bound and there is a clear trade-off between spectral bandwidth and achievable enhancement. These spectra represent the theoretical limit of photocurrent enhancement that can be achieved using the planar coherent light-trapping technique that can be physically implemented using discrete refractive index multilayer coatings or as planar graded index structures.

Figure 4(a) shows the achievable average AM 1.5-weighted EQE for the BHJ device using mirrors that satisfy the SSKK-constraint for the full absorption band as a function of the active layer thickness (solid triangles) for critical lengths of charge collection  $L_c=20\text{nm}$  and  $40\text{nm}$ . The average EQE for a control device without dielectric mirror is also shown for reference (open triangles). Despite the limits imposed by Eq. (7), optical interference effects can be used to trap light and improve the photocurrent produced by a thin-film solar cell. For the  $15\text{nm}$ -thick BHJ device, the model predicts an increase in short-circuit current density from  $3.2\text{mA}/\text{cm}^2$  for the control device to  $4.9\text{mA}/\text{cm}^2$  when the SSKK-consistent mirror is included, representing a 53% increase. The achievable enhancement in AM1.5-weighted average EQE as a function of active layer thickness is also shown (circles). As expected, the thinnest device structures benefit most from light trapping.

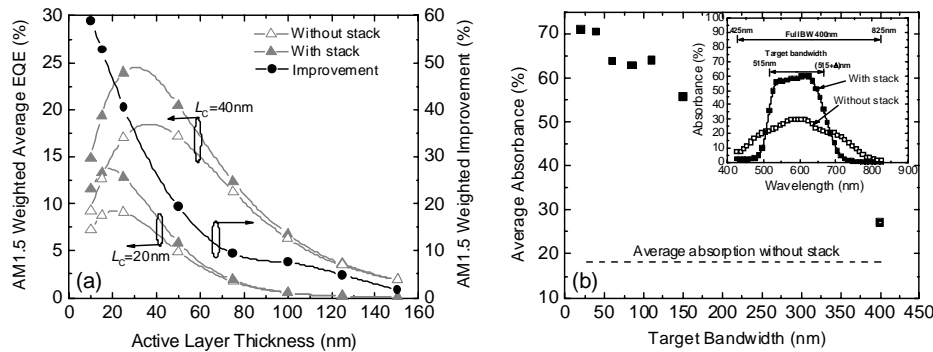


Fig. 4. (a). AM1.5-weighted average EQE for the control BHJ device (open triangles) and a BHJ device with an optimal causal top mirror (filled triangles) for different charge collection lengths ( $L_c=20\text{nm}$  and  $40\text{nm}$ ) as a function of the thickness of active layer. Also shown is the broadband improvement achieved through coherent light trapping as a function of the active layer thickness. (b). Optimal causal limit of absorbance averaged over the spectral range  $\lambda=425\text{nm}-825\text{nm}$  that is achievable as a function of the targeted bandwidth for a device with  $15\text{nm}$ -thick active layer. Inset: Example of an absorbance spectrum without stack (open squares) and with stack (solid squares) optimized for a bandwidth of  $150\text{nm}$ .

Figure 4(b) shows the average absorption (averaged for the spectral range  $\lambda=425\text{nm}-825\text{nm}$ ) as a function of the bandwidth over which absorption enhancement is desired for the BHJ device with a  $15\text{nm}$ -thick active layer. Structures with a tuned mirror that absorb  $\sim 56\%$  of the incident power within a  $150\text{nm}$  bandwidth are physically realizable [see inset to Fig. 4(b)], despite the mirrorless structure only absorbing  $28\%$  over the same bandwidth. While  $150\text{nm}$  is narrow compared to the solar spectrum, the enhancement of the absorption in well-defined spectral bands might be useful in tandem configurations where separate cells are used for different spectral regions [34].

We now present a practical numerical optimization scheme to design two-component dielectric stacks with characteristics that approach the limit set by the SSKK relation. It has been shown that two-component coatings with the maximum and minimum refractive indices

available are optimal coatings [35]. The stacks use  $\text{SiO}_2$  ( $n=1.5$ ) and  $\text{TiO}_2$  ( $n=2.5$ ) as the low and high-index material, respectively. The optimization procedure targets to achieve maximum photocurrent averaged over s and p polarizations and over a whole 12-hour day. The spectrum is assumed to be the AM1.5 spectrum whose intensity varies as the cosine of the incident angle. The optimization routine starts with a thin-film organic PV cell with a single thick dielectric layer of  $\text{SiO}_2$  inserted between the glass substrate and ITO electrode. An exhaustive search is then performed for the optimal location for the insertion of a new layer [36]-[39]. Since characteristic matrices are stored, this exhaustive search only requires the calculation of three additional characteristic matrices for each tested structure. Repeated insertion of layers is performed before a Nelder-Mead simplex algorithm [40] is used to find a locally optimal set of layer thicknesses. The design is automatically purged of any layers less than 6nm thick. This procedure is repeated with different thicknesses and different numbers of simultaneous new layer insertions. The optimization ends when the desired performance is achieved or if no further layers can be increased without degrading performance. If the desired performance is not achieved, the overall coating thickness may be increased to enable further layer insertions. A similar optimization procedure was previously developed [38] and experimentally verified [39] by the authors for applications in organic light emitting diodes. The present optimization scheme was implemented in a commercial linear algebra package [41]. The results of design procedure are a 4-layer design for the BHJ cell and a 6-layer design for the bilayer cell. The resulting stack designs are shown in Table 1.

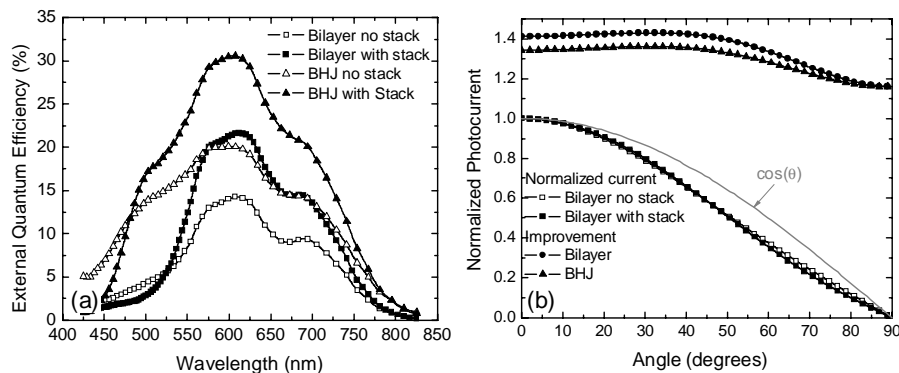


Fig. 5. (a). External quantum efficiency for the bilayer (squares) and the BHJ (triangles) 15nm-thick cells with (filled symbols) and without (open symbols) an optimized dielectric stack between the substrate and ITO layer. (b) Normalized short-circuit current as a function of angle of incidence of the illumination for a 15nm-thick bilayer device with (filled squares) and without (open squares) an optimized dielectric stack. The short circuit current at normal incidence is normalized to 1. The enhancement in short-circuit current density by insertion of the optimized dielectric stack is also shown for the bilayer (circles) and the BHJ (triangles) devices.

Figure 5(a) shows the modeled external quantum efficiency at normal incidence for the bilayer (squares) and the BHJ (triangles) cell with (solid symbols) and without (open symbols) the dielectric mirrors. The charge collection efficiency was assumed to be 100% since we are interested in the achievable enhancement. The optimization scheme resulted in a decrease in response at short wavelengths and an enhancement in response for longer wavelengths to match the cell response to the solar spectrum. This is an example of a redistribution of the PDOS to achieve better performance. The short-circuit current density under AM1.5 illumination increases from  $2.6\text{mA}/\text{cm}^2$  to  $3.7\text{mA}/\text{cm}^2$  for the bilayer cell (a 42% enhancement), and from  $3.2\text{mA}/\text{cm}^2$  to  $4.3\text{mA}/\text{cm}^2$  for the BHJ cell (a 34% enhancement). The effects described here were observed in a simplified structure where a single dielectric layer was used to increase the monochromatic photocurrent in an organic thin-film solar cell

by 30% [42]. The methods presented here provide a larger and spectrally broader enhancement.

Figure 5(b) shows the dependence of normalized short-circuit current density on the angle of incidence,  $\theta$ , for the bilayer cells with (filled squares) and without (open squares) an optimized dielectric stack. The short-circuit current density is normalized to unity at normal incidence. The interference coating does not result in a strong dependence of short-circuit current density on  $\theta$ . Both with and without dielectric stack, short circuit current approximately follows a  $\cos(\theta)$ -dependence because the optical flux varies as  $\cos(\theta)$  (grey line). The enhancement achieved in the short-circuit current density as a function of azimuthal angle by inclusion of the dielectric stacks for the bilayer (filled circles) and the BHJ (filled triangles) cell, is also shown. At normal incidence, a 42% and 34% improvement in short-circuit current density is obtained for the bilayer and BHJ cell, respectively. For angles  $>50^\circ$  the enhancement decreases rapidly. The optimization procedure automatically optimized for angles near normal incidence since the optical flux falls off as  $\cos(\theta)$ . The enhancement in photocurrent averaged over a full day is 40% and 33% for the bilayer and BHJ cell, respectively.

In conclusion, we have shown that specifically designed dielectric mirrors can be used to substantially enhance the optical absorption in thin-film PV cells by modifying the PDOS. These dielectric mirrors are a generalization of ARCs and mirrors for RCE photodetectors. Using thin-film organic PV cell model systems, we have shown that enhancements in photocurrent of up to 40% are achievable despite a broadband absorption spectrum. With low-cost techniques to manufacture such thin-film dielectric coatings, this approach may be of practical use to enhance the efficiency of thin-film solar cells.

#### **Acknowledgment**

This work was partially supported by the Stanford Global Climate and Energy Project and AFOSR #FA9550-06-1-0399.